

# Projected shell model study of odd-odd $f$ - $p$ - $g$ shell proton-rich nuclei

R. Palit<sup>1,2</sup>, J.A. Sheikh<sup>3</sup>, Y. Sun<sup>4,5,6</sup> and H.C. Jain<sup>1</sup>

<sup>(1)</sup>*Tata Institute of Fundamental Research, Mumbai 400 005, India*

<sup>(2)</sup>*Institut für Kernphysik, Johann Wolfgang Goethe Universität, D-60486 Frankfurt, Germany*

<sup>(3)</sup>*Physik-Department, Technische Universität München, D-85747 Garching, Germany*

<sup>(4)</sup>*Department of Physics and Astronomy, University of Tennessee, Knoxville, Tennessee 37996, U.S.A.*

<sup>(5)</sup>*Department of Physics, Tsinghua University, Beijing 100084, P.R. China*

<sup>(6)</sup>*Department of Physics, Xuzhou Normal University, Xuzhou, Jiangsu 221009, P.R. China*

---

## Abstract

A systematic study of 2-quasiparticle bands of the proton-rich odd-odd nuclei in the mass  $A \sim 70 - 80$  region is performed using the projected shell model approach. The study includes Br-, Rb-, and Y-isotopes with  $N = Z$ ,  $Z+2$ , and  $Z+4$ . We describe the energy spectra and electromagnetic transition strengths in terms of the configuration mixing of the angular-momentum projected multi-quasiparticle states. Signature splitting and signature inversion in the rotational bands are also discussed. The deficiency of the model in the description of  $N = Z$  systems is pointed out.

---

PACS: 21.60Cs;21.10.Ky;21.10.Re

Keywords: Electromagnetic transition strength; Angular momentum projection;

## 1 Introduction

Deformed odd-odd nuclei provide valuable information on the interplay between the collective and the single-neutron and -proton degrees of freedom in atomic nuclei. In general, odd-odd nuclei are difficult to study both experimentally and theoretically due to the complexity of their low-lying spectra. In

comparison to even-even nuclei where the pairing correlations favor a particular configuration, in odd-odd nuclei many configurations are equally probable, and therefore, contribute to the complexity of the spectra. A detailed experimental analysis for the odd-odd nuclei with mass  $A \sim 70 - 80$  has become possible only in the last few years with the availability of large arrays of high resolution HPGe detectors. Some extensive measurements of the proton-rich odd-odd nuclei [1–12] have been carried out for the Br-, Rb- and Y-isotopes in laboratories around the world. The excited states of some of these nuclei have been populated upto high-spins, e.g.  $I \approx 20\hbar$ , by heavy-ion fusion reactions. In each of these nuclei several bands have been established. The low-lying levels of these bands show very irregular behavior, whereas at moderate rotational-frequency, i.e.  $\hbar\omega \approx 0.5$  MeV, regular rotational bands start developing. The stretched  $E2$  transition strengths deduced from measured lifetimes of excited states indicate higher degree collectivity for the high-spin states. Furthermore, a considerable amount of odd-even staggering (signature splitting) in transition energies is observed in these bands. In some of them, the staggering phase shows an inversion at spin  $I \approx 10$ .

The study of these proton-rich nuclei is not only interesting from the nuclear structure point of view, but also has important implications in nuclear astrophysics [13]. Since heavier elements are made in stellar evolution and explosions, nuclear physics, and in particular nuclear structure far from stability, enters into the stellar modeling in a crucial way. It is believed that these proton-rich nuclei near the  $N = Z$  line are synthesised in the rapid-proton capture process (the rp-process) under appropriate astrophysical conditions. The X-ray burst is suggested as a possible site. Recently, the proton-rich odd-odd nuclei with  $A \sim 70 - 80$  have been studied more rigorously partially due to this astrophysical interest. Understanding the structure of the low-lying states in these nuclei is also important for the study of Fermi superallowed  $\beta^+$  decays [14].

On the theoretical front, very little effort has been put in the study of doubly odd nuclei as compared to even-even nuclei in this mass region. The microscopic calculations based on the Excited-VAMPIR approach [15,16] were performed for some odd-odd nuclei. The large-scale spherical shell model [17] which is quite successful for describing the  $pf$ -shell nuclei, can not be applied for these well-deformed mass-80 nuclei since it is important to include the  $g$ -shell. The configuration space required for such a study is quite enormous and can not be handled by the present state-of-the-art computational facilities.

In recent years, the projected shell model (PSM) [18] has become quite successful in explaining a broad range of properties of deformed nuclei in various regions of the nuclear periodic-table. The most striking aspect of this quantum mechanical model is its ability to describe the finer details of the high-spin spectroscopy data with simple physical interpretations. The studies of odd-odd

rare-earth nuclei [19] have shown this capability. Very recently, the PSM has been systematically applied to the even-even Kr-, Sr-, and Zr-isotopes of the proton-rich region[20], where it has been found that the PSM results are able to explain most of the experimental observations. The purpose of the present work is to carry out a similar study for the proton-rich, odd-odd Br-, Rb- and Y-isotopes with  $N = Z+2$  and  $Z+4$ , and with an example of  $N = Z$  nucleus. The physical quantities to be described are energy spectrum and electromagnetic transition probability. A quantitative comparison of calculated and measured transition strengths can provide a stringent test of the model. We would like to mention here that the present study is the first major application of the projected shell model approach to the medium mass odd-odd nuclei. It is also for the first time that calculations for the electromagnetic transition strengths in odd-odd nuclei are performed within the PSM framework.

The manuscript is organized as follows: In the next section, we shall give a brief outline of the model for completeness. This section also gives expressions for various physical quantities to be discussed in this paper. The results of calculations and comparisons with the experimental data are presented in Section 3. Finally, a summary is given in Section 4.

## 2 The projected shell model

In the projected shell model approach the basis in which the shell model Hamiltonian is diagonalised, is chosen in the quasi-particle (qp) space. For odd-odd nuclei, the ground-band is a two quasi-particle configuration and in order to describe the structure of a well-deformed odd-odd nuclei, it is necessary to consider atleast two qp configurations in the basis. As a matter of fact, due to the Pauli blocking of levels, quite upto high-spins these two qp configurations are sufficient to describe the physics. Thus, for low-lying bands of odd-odd nuclei, the quasiparticle configuration space consists of a set of 2-qp states

$$\{|\phi_\kappa\rangle = a_\nu^\dagger a_\pi^\dagger |0\rangle\}. \quad (1)$$

The qp-vacuum  $|0\rangle$  is determined by diagonalization of a deformed Nilsson Hamiltonian and a subsequent BCS calculations. This defines the Nilsson + BCS qp-basis. Here, the quantum numbers for neutron ( $\nu$ ) and proton ( $\pi$ ) run over the Nilsson single-particle states near the respective Fermi levels. The configuration space is obviously large in this case compared to the nearby odd-mass nuclei, and usually several configurations contribute to the shell model wave function of a state with nearly equal weightage. This makes the numerical results very sensitive to the shell filling and the theoretical predictions for

doubly-odd nuclei become far more challenging.

The states  $|\phi_\kappa\rangle$  obtained from the deformed Nilsson calculations do not conserve rotational symmetry. To restore this symmetry, angular-momentum projection technique is applied. The effect of rotation is totally described by the angular-momentum projection operator and the whole dependence of wave functions on spin is contained in the eigenvectors, since the Nilsson quasi-particle basis is not spin-dependent. From each intrinsic state in (1) a band can be generated by projection. The interaction between different bands with a given spin is taken into account by diagonalising the shell model Hamiltonian in the projected basis.

The Hamiltonian used in the present work is

$$\hat{H} = \hat{H}_0 - \frac{1}{2}\chi \sum_{\mu} \hat{Q}_{\mu}^{\dagger} \hat{Q}_{\mu} - G_M \hat{P}^{\dagger} \hat{P} - G_Q \sum_{\mu} \hat{P}_{\mu}^{\dagger} \hat{P}_{\mu}, \quad (2)$$

where  $\hat{H}_0$  is the spherical single-particle shell model Hamiltonian. The second, third and fourth terms represent quadrupole-quadrupole, monopole-pairing, and quadrupole-pairing interactions, respectively. The strength of the quadrupole-quadrupole force  $\chi$  is determined in such a way that the employed quadrupole deformation  $\epsilon_2$  (see Table I) is same as obtained by the HFB procedure. The monopole-pairing force constants  $G_M$  used in the calculations are

$$G_M^{\nu} = [20.25 - 16.20 \frac{N-Z}{A}] A^{-1}, \quad G_M^{\pi} = 20.25 A^{-1}. \quad (3)$$

Finally, the quadrupole pairing strength  $G_Q$  is assumed to be proportional to the monopole strength,  $G_Q = 0.16G_M$ . All these interaction strengths are the same as those in our previous calculations for the even-even nuclei of the same mass region [20,21]. Thus, we have a consistent description for doubly-even and doubly-odd nuclear systems.

Once the projected basis is prepared, we diagonalize the Hamiltonian in the shell model space spanned by  $\hat{P}_{MK}^I |\phi_\kappa\rangle$ . So, the ansatz for the wave function is given by

$$|\sigma, IM\rangle = \sum_{K,\kappa} f_{\kappa}^{\sigma} \hat{P}_{MK}^I |\phi_{\kappa}\rangle. \quad (4)$$

Here, the index  $\sigma$  labels the states with same angular momentum and  $\kappa$  the basis states.  $\hat{P}_{MK}^I$  is angular momentum projection operator and  $f_{\kappa}^{\sigma}$  are the weights of the basis state  $\kappa$ . This leads to the eigenvalue equation

$$\sum_{\kappa'} (H_{\kappa\kappa'} - E_{\sigma} N_{\kappa\kappa'}) f_{\kappa'}^{\sigma} = 0, \quad (5)$$

and the normalization is chosen such that

$$\sum_{\kappa\kappa'} f_{\kappa}^{\sigma} N_{\kappa\kappa'} f_{\kappa'}^{\sigma'} = \delta_{\sigma\sigma'}. \quad (6)$$

The angular-momentum-projected wave functions are laboratory wave functions and can thus be directly used to compute the observables. The reduced electric quadrupole transition probability  $B(E2)$  from an initial state  $(\sigma_i, I_i)$  to a final state  $(\sigma_f, I_f)$  is given by [22]

$$B(E2, I_i \rightarrow I_f) = \frac{e^2}{2I_i + 1} |\langle \sigma_f, I_f | \hat{Q}_2 | \sigma_i, I_i \rangle|^2. \quad (7)$$

In the calculations, we have used the effective charges of 1.6e for protons and 0.6e for neutrons. The reduced magnetic dipole transition probability  $B(M1)$  is computed by

$$B(M1, I_i \rightarrow I_f) = \frac{\mu_N^2}{2I_i + 1} |\langle \sigma_f, I_f | \hat{\mathcal{M}}_1 | \sigma_i, I_i \rangle|^2, \quad (8)$$

where the magnetic dipole operator is defined as

$$\hat{\mathcal{M}}_1^{\tau} = g_l^{\tau} \hat{j}^{\tau} + (g_s^{\tau} - g_l^{\tau}) \hat{s}^{\tau}. \quad (9)$$

Here,  $\tau$  is either  $\nu$  or  $\pi$ , and  $g_l$  and  $g_s$  are the orbital and the spin gyromagnetic factors, respectively. In the calculations we use for the  $g_l$  the free values and for  $g_s$  the free values damped by a 0.85 factor

$$g_l^{\pi} = 1, \quad g_l^{\nu} = 0, \quad g_s^{\pi} = 5.586 \times 0.85, \quad g_s^{\nu} = -3.826 \times 0.85. \quad (10)$$

Since the configuration space is large enough we do not use any core contribution. More concretely, the reduced matrix element  $\hat{\mathcal{O}}$  ( $\hat{\mathcal{O}}$  is either  $\hat{Q}$  or  $\hat{\mathcal{M}}$ ) is expressed by

$$\begin{aligned} \langle \sigma_f, I_f | \hat{\mathcal{O}}_L | \sigma_i, I_i \rangle &= \sum_{\kappa_i, \kappa_f} f_{I_i \kappa_i}^{\sigma_i} f_{I_f \kappa_f}^{\sigma_f} \sum_{M_i, M_f, M} (-)^{I_f - M_f} \begin{pmatrix} I_f & L & I_i \\ -M_f & M & M_i \end{pmatrix} \\ &\quad \langle \phi_{\kappa_f} | \hat{P}_{K_{\kappa_f} M_f}^{I_f} \hat{\mathcal{O}}_{LM} \hat{P}_{K_{\kappa_i} M_i}^{I_i} | \phi_{\kappa_i} \rangle \end{aligned} \quad (11)$$

### 3 Results and discussions

For  $N = Z+2, Z+4$  isotopes of odd-odd Br, Rb, and Y, the  $\pi g_{9/2} \otimes \nu g_{9/2}$ , 2qp configuration has been firmly established for the yrast region. This configuration has been observed up to or above 10 MeV excitation energy in these nuclei. Therefore, we first discuss the calculations for these nuclei in the following three subsections. The discussion includes the band diagrams, transition energies and electromagnetic transition strengths (the  $B(M1)$  and  $B(E2)$  values) of each of the above mentioned isotopes.

The odd-odd  $N = Z$  nuclei of this mass region appear to have a different structure as compared to the neighbouring nuclei. Experimentally, the odd-odd  $N = Z$  nuclei are far more difficult to study since they lie further away from the stability valley, approaching the proton drip-line. For the few measured cases [1,2,6], both the low-spin and high-spin states exhibit distinct properties. The structure with the presence of the isospin,  $T = 1$  and  $T = 0$  bands is further complicated by the prolate-oblate shape co-existence. Theoretically, most of the structure models do not treat explicitly the isospin degree of freedom, which describes the neutron-proton exchange symmetry. The current version of the PSM belongs to this category. Therefore, states with isospin symmetry and isospin anti-symmetry cannot be described by the PSM at present. Nevertheless, we discuss an example of the experimentally known  $N = Z$  nucleus  $^{74}\text{Rb}$  [6] to see the applicability and limitation of this simple model.

The PSM calculations proceed in two steps. First, an optimum set of deformed basis is constructed from the standard Nilsson model. The Nilsson parameters are taken from Ref. [23] and the calculations are performed by considering three major shells ( $N = 2, 3$  and  $4$ ) for both neutrons and protons. The basis deformation  $\epsilon_2$  used for each nucleus is given in Table I. These values are taken either according to experimental information, if available, or from theoretical calculations. We emphasize that unlike the cranking mean field approaches, the deformation parameters used as an input to the PSM calculations need not correspond exactly to the true nuclear deformation. This is because of the shell-model nature of the PSM: The deformed single-particle states serve solely as a way to truncate shell-model basis. All observable properties in the PSM calculations are determined by the many-body wave-functions obtained by diagonalising the shell model Hamiltonian. In principle, the larger the deviation of the initial deformation from the true one, the bigger will be the configuration space for an actual description of the nuclei. In the present calculations, the space is truncated by the inclusion of the states within an energy window of 3.5 MeV around the Fermi surface. This determines the size of the basis space,  $|\phi_\kappa\rangle$  in Eq. (1), of the order of 30. In the second step, these basis states are projected to good angular momentum states, and the projected basis is

then used to diagonalize the shell model Hamiltonian. The diagonalization gives rise to the energy spectra, and the transition strengths are subsequently calculated using the resulting wave functions.

### 3.1 Band diagram

For the deformation values given in Table I, the  $[440]\frac{1}{2}$ ,  $[431]\frac{3}{2}$ ,  $[422]\frac{5}{2}$  orbitals for protons and neutrons lie near the Fermi surfaces in the nuclei under consideration. To describe the low-lying structure of these nuclei, the 2-qp states based on these orbitals (with  $K = K_\nu \pm K_\pi$ ) should be taken into account. A representative band diagram for  $^{74}\text{Br}$ , containing some unperturbed rotational bands, is shown in Fig. 1 to see the underlying structure. Note that only the important configurations are displayed in the band diagram, although many more others are included in the calculations.

Out of the all unperturbed bands taken in the diagonalization, only few of them show energy staggering between odd- and even-spin states (the so-called signature splitting). As can be seen in Fig. 1, these bands have the zigzag behavior as a function of spin. This occurs for the bands with configurations involving low- $K$  orbitals. It was noticed in Ref. [19] that unlike in the particle rotor model, the configurations based on orbitals with  $K \neq \frac{1}{2}$  also contribute to the energy staggering. The unperturbed bands which show staggering influence the yrast states through the band mixing, and thus cause the signature dependence in the yrast band (shown as filled circles in Fig. 1). It is seen from Fig. 1 that the lowest  $K = 4$  band has only small staggering. The clear signature splitting at around spin  $I = 10$  come mainly from the mixing of the 2-qp band based on  $(\nu[431]\frac{3}{2} \otimes \pi[431]\frac{3}{2})$ . Two more pairs of bands with  $K = 1, 2$  based on  $(\nu[431]\frac{3}{2} \otimes \pi[440]\frac{1}{2})$  and  $K = 1, 0$  based on  $(\nu[440]\frac{1}{2} \otimes \pi[440]\frac{1}{2})$  have much stronger signature splitting. They dive down to the yrast region at higher spins, and therefore bring strong energy staggering to the yrast band. It is thus the configuration mixing that produces nicely the observed signature splitting as one will see in Fig. 2 below.

Interestingly, the current PSM calculations indicate that the phase of the energy staggering may change at certain spins. In Fig. 1, two of the above mentioned bands with  $K = 0$  based on  $(\nu[440]\frac{1}{2} \otimes \pi[440]\frac{1}{2})$  and  $K = 1$  based on  $(\nu[431]\frac{3}{2} \otimes \pi[440]\frac{1}{2})$  show an inversion in the staggering phase (the so-called signature inversion). The inversion appears at  $I = 6$  for the former, and  $I = 10$  for the latter. Note that this is a signature inversion occurring within one unperturbed band, without involving any dynamic mixture with other bands. Hara and Sun called this kind of inversion a self-inversion, to distinguish this from an inversion involving two bands with mutually opposite staggering phases [19]. The phenomenon of self-inversion predicted in Ref.

[19] has not been confirmed experimentally. Here, the band with self-inversion (emphasized by a solid bold curve at  $I = 8 - 11$  in Fig. 1) lies at very low excitations and the inversion appears at spin  $I \approx 10$ . This is a promising candidate that may explain the observed signature inversion in the rotational band in  $^{74}\text{Br}$  [4] and other nuclei in this mass region.

### 3.2 Transition energies

After diagonalization at each spin, the lowest energies give the energies of the yrast states. The energy differences between adjacent spin states are compared with the measured transition energies in Fig. 2 for  $^{72,74}\text{Br}$ ,  $^{76,78}\text{Rb}$  and  $^{80,82}\text{Y}$ . The characteristic feature of the six nuclei is the exhibition of a clear energy staggering between the odd- and even-spin states, as seen in the  $E(I) - E(I-1)$  plot in Fig. 2. It is called signature splitting because the odd- and even-spin states can be classified as two groups specified by the signature quantum number. In addition, an inversion in the staggering phase is observed in most of the nuclei. Signature inversion in the mass-80 region was discussed in Ref. [24].

As can be seen from Fig. 2, for all of the nuclei the agreement between the calculation and experiment is quite satisfactory above  $I \approx 10\hbar$ . The energy splitting at higher spins is well reproduced in all the cases, indicating that the important influence on the yrast band from the low- $K$  components of the  $g_{9/2}$  valance neutrons and protons are correctly accounted for by the configuration mixing.

However, the calculation does not reproduce the signature inversion observed at low spins in  $^{74}\text{Br}$ ,  $^{76,78}\text{Rb}$  and  $^{80,82}\text{Y}$ . This is rather unfortunate because the mechanism that may cause the inversion is clearly present in the model. In this medium mass region with  $N \sim Z$ , rotational bands with mutually opposite signature dependence can not co-exist near the yrast region, and therefore, the only possibility to explain the observed signature inversion is through the self-inversion. In Ref. [19], the favorite condition for this to happen was given to nuclei where bands based on configurations with  $K = 0$  ( $\nu K = \frac{1}{2} \otimes \pi K = \frac{1}{2}$ ) and  $K = 1$  ( $\nu K = \frac{3}{2} \otimes \pi K = \frac{1}{2}$ ) lie low in energy.  $^{74}\text{Br}$  fulfils these conditions. The failure that our final results do not reproduce the signature inversion may indicate that the band mixing is not strong enough to bring the desired feature of self-inversion into the yrast band. One may generally argue that there should be an interaction that particularly pushes the unperturbed band with self-inversion further down to affect the yrast states more strongly. Obviously, this force is absent in the schematic Hamiltonian employed in the current model.

### 3.3 Electromagnetic transition strengths

The experimental data from lifetime measurements performed for  $^{74}\text{Br}$ ,  $^{78}\text{Rb}$  and  $^{82}\text{Y}$  [4,5,8,9,12] have separately provided the  $B(\text{M1})$  and  $B(\text{E2})$  values. For  $^{72}\text{Br}$  and  $^{76}\text{Rb}$ , no lifetime measurements have been performed: the ratio  $B(\text{M1})/B(\text{E2})$  could be obtained from the measured intensity of transitions. In the present section, these data are compared with our calculations.

The experimental  $B(\text{M1})$  values for  $^{74}\text{Br}$ ,  $^{78}\text{Rb}$  and  $^{82}\text{Y}$  are plotted in Fig 3. In all the three nuclei, staggering between the odd- and even-spin states is clearly present. This variation in the  $B(\text{M1})$  pattern is directly compared with the calculated transition strengths. Except for a few particular states, the calculation achieves a quantitatively agreement with data. In contrast to the transition energies, no inversion in the staggering phase is obtained in both theory and experiment. The measured  $B(\text{E2})$  values for  $^{74}\text{Br}$ ,  $^{78}\text{Rb}$  and  $^{82}\text{Y}$  are plotted in Fig. 4. The global trend of the  $B(\text{E2})$  curve as a function of spin is qualitatively reproduced by the calculation as shown in the Fig. 4, although some deviations are seen at high spins.

In Fig. 5, the calculated  $B(\text{M1})/B(\text{E2})$  values are compared with the experimental data wherever available for  $^{72}\text{Br}$ ,  $^{76}\text{Rb}$  and  $^{80}\text{Y}$ . A staggering pattern is again observed in experimentally deduced  $B(\text{M1})/B(\text{E2})$  ratios for those levels for which cascade M1 transitions have been observed. Indeed, in  $^{72}\text{Br}$   $B(\text{M1})/B(\text{E2})$  values for the  $11^{(+)}$  and  $13^{(+)}$  levels are  $\approx 10 \mu_n^2/(eb)^2$ , while for  $10^{(+)}$  level its value is only  $0.03(1) \mu_n^2/(eb)^2$  [3]. These features are quite nicely reproduced by the calculation. The experimental ratio  $B(\text{M1})/B(\text{E2})$  in  $^{76}\text{Rb}$  were determined from the measured intensity of transitions reported in Ref. [7]. The  $B(\text{M1})/B(\text{E2})$  values in  $^{76}\text{Rb}$  are generally smaller compared to the ratio observed in  $^{72}\text{Br}$ . This fact reflects the smaller contribution from the lower K orbitals for  $^{76}\text{Rb}$ . Unfortunately, in case of  $^{80}\text{Y}$  no intensities for different transitions in the positive parity band is available to allow a determination of the  $B(\text{M1})/B(\text{E2})$  ratios experimentally. The calculated values of  $B(\text{M1})/B(\text{E2})$  ratio are small compared to those of  $^{72}\text{Br}$  and  $^{76}\text{Rb}$ .

### 3.4 The $N = Z$ nucleus $^{74}\text{Rb}$

In Ref. [6], two rotational bands were observed in the  $N = Z$  nucleus  $^{74}\text{Rb}$ . In contrast to the above discussed  $N = Z+2$  and  $Z+4$  nuclei, the ground-state band of  $^{74}\text{Rb}$  does not look like a rotational band having the usual 2-qp structure. Instead, the transition energies of the ground state band in  $^{74}\text{Rb}$  show similarities to those in even-even nuclei. In fact, they have been interpreted [6] as being formed from the  $T = 1$  isobaric analog states of  $^{74}\text{Kr}$

with pairing correlations based on  $T = 1$  neutron-proton pairs. At higher rotational frequency, a  $T = 0$  rotational band becomes energetically favored over the  $T = 1$  ground state band.

Obviously, a full description for these observations is not possible in the present version of the PSM since the physics is beyond what the model space in (1) can provide. However, using the concept of spontaneous breaking of the isospin invariance, in ref. [25] it was argued that the neutron-proton interaction can be effectively considered in a theory with only neutron-neutron and proton-proton pairings, since one has a freedom to choose a one particular direction in the isospin space. One thus ends up with the understanding that the  $T = 1$  ground state band in an odd-odd  $N = Z$  nucleus may be approached by a 0-qp state with nn and pp pairings and the  $T = 0$  rotational band has a structure similar to the 2-qp states [25].

The two neighboring even-even  $N = Z$  nuclei  $^{72}\text{Kr}$  and  $^{76}\text{Sr}$  have a large deformation with  $\epsilon_2 \approx 0.36$  [20,21]. It is thus reasonable to perform a calculation for  $^{74}\text{Rb}$  with this deformation. At the deformation  $\epsilon_2 = 0.36$ , the  $[422]\frac{5}{2}^+$  orbital is the closest to the respective neutron and proton Fermi levels in  $^{74}\text{Rb}$ . Thus, the band based on the 2-qp state of  $K = 5$  ( $\nu[422]\frac{5}{2}^+ \otimes \pi[422]\frac{5}{2}^+$ ) is the lowest in energy among all the 2-qp states (see Fig. 6). At higher spins, bands consist of smaller  $K$ -states  $[440]\frac{1}{2}^+$ ,  $[431]\frac{3}{2}^+$ , which show stronger signature splitting, mix with the  $K = 5$  band through configuration mixing. Therefore, the mixed band follows the signature phase that favors the odd-spin states. This may explain the absence of even spin states in the experimental spectra at the high spin region [6].

In Fig. 7, the two observed rotational bands in  $^{74}\text{Rb}$  are compared with the calculations in an  $E(I) - E(I-2)$  plot. It is seen that the calculated results fit the data reasonably well. This indicates that the physical understanding of ref. [25] on the band structure in an odd-odd  $N=Z$  nucleus is correct. However, in order to understand the interplay between the  $T=0$  and 1 bands, it is necessary to include the neutron-proton pairing in the shell model Hamiltonian.

## 4 Summary

In the present manuscript, we have performed a systematic study for the positive parity yrast bands of odd-odd nuclei  $^{72,74}\text{Br}$ ,  $^{76,78}\text{Rb}$  and  $^{80,82}\text{Y}$  using the projected shell model approach. Furthermore, an  $N = Z$  nucleus  $^{74}\text{Rb}$  has also been studied. We discussed many features observed in these nuclei using the angular-momentum projected 2-quasiparticle states with the employment of a simple quadrupole-quadrupole + monopole-pairing + quadrupole-pairing Hamiltonian. The neutron-proton interaction is present only in the

particle-hole channel. We have pointed out the successes and inadequacies of the projected shell model approach in explaining the odd-odd nuclei with mass  $A \sim 70 - 80$ . The main feature that both transition energies and electromagnetic transition strengths show a staggering pattern has been successfully described by the model in terms of configuration mixing. In general, a good agreement between the experimental data and calculated values has been found in the high-spin region, but there are discrepancies in the low-spin domain. This indicates that in the high-spin region, the nuclei studied acquire a stable deformation, which is the original idea in the development of the projected shell model approach. The disagreement in the low-spin region can be attributed to the shape-coexistence and the vibrational degree of freedom, which are not considered in the present approach.

Finally, we conclude with the note that in order to study a deformed odd-odd  $N = Z$  system in an adequate manner, the current model needs to be improved with angular-momentum projection on an extended quasiparticle basis that allows for a mixing of proton and neutron single-particle states. The work along these lines is in progress and will be reported in the near future.

## References

- [1] G. de Angelis, T. Martinez, A. Gadea, N. Marginean, E. Farnea, E. Maglione, S. Lenzi, W. Gelletly, C.A. Ur, D.R. Napoli, Th. Kroell, S. Lunardi, B. Rubio, M. Axiotis, D. Bazzacco, A.M. Bizzeti Sona, P.G. Bizzeti, P. Bednarczyk, A. Bracco, F. Brandolini, F. Camera, D. Curien, M. De Poli, O. Dorvaux, J. Eberth, H. Grawe, R. Menegazzo, G. Nardelli, J. Nyberg, P. Pavan, B. Quintana, C. Rossi Alvarez, P. Spolaore, T. Steinhart, I. Stefanescu, O. Thelen, and R. Venturelli, *Eur. Phys. J. A*12, 51 (2001).
- [2] D.G. Jenkins, N.S. Kelsall, C.J. Lister, D.P. Balamuth, M.P. Carpenter, T.A. Sienko, S.M. Fischer, R.M. Clark, P. Fallon, A. Görgen, A.O. Macchiavelli, C.E. Svensson, R. Wadsworth, W. Reviol, D.G. Sarantites, G.C. Ball, J. Rikovska Stone, O. Juillet, P. Van Isacker, A.V. Afanasjev, and S. Frauendorf, *Phys. Rev. C*65, 064307 (2002).
- [3] N. Fotiades, J.A. Cizewski, C.J. Lister, C.N. Davids, R.V.F. Janssens, D. Seweryniak, M.P. Carpenter, T.L. Khoo, T. Lauritsen, D. Nisius, P. Reiter, J. Uusitalo, I. Wiedenhöver, A.O. Macchiavelli, and R.W. MacLeod, *Phys. Rev. C*60, 057302 (1999).
- [4] G. Garcia-Bermudez, M.A. Cardona, A. Filevich, R.V. Ribas, H. Somacal, and L. Szybisz, *Phys. Rev. C*59, 1999 (1999).
- [5] J.W. Holcomb, T.D. Johnson, P.C. Womble, P.D. Cottle, S.L. Tabor, F.E. Durham, and S.G. Buccino, *Phys. Rev. C*43, 470 (1991).

- [6] D. Rudolph, C.J. Gross, J.A. Sheikh, D.D. Warner, I.G. Bearden, R.A. Cunningham, D. Foltescu, W. Gelletly, F. Hannachi, A. Harder, T.D. Johnson, A. Jungclaus, M.K. Kabadiyski, D. Kast, K.P. Lieb, H.A. Roth, T. Shizuma, J. Simpson, Ö. Skeppstedt, B.J. Varley, and M. Weiszflog, *Phys. Rev. Lett.* 76, 376 (1996).
- [7] A. Harder, M.K. Kabadiyski, K.P. Lieb, D. Rudolph, C.J. Gross, R.A. Cunningham, F. Hannachi, J. Simpson, D.D. Warner, H.A. Roth, Ö. Skeppstedt, W. Gelletly, and B.J. Varley, *Phys. Rev. C*51, 2932 (1995).
- [8] R.A. Kaye, J. Döring, J.W. Holcomb, G.D. Johns, T.D. Johnson, M.A. Riley, G.N. Sylvan, P.C. Womble, V.A. Wood, S.L. Tabor, and J.X. Saladin, *Phys. Rev. C*54, 1038 (1996).
- [9] R.A. Kaye, L.A. Riley, G.Z. Solomon, S.L. Tabor, and P. Semmes, *Phys. Rev. C*58, 3228 (1998).
- [10] J. Uusitalo, D. Seweryniak, P.F. Mantica, J. Rikovska, D.S. Brenner, M. Huhta, J. Greene, J.J. Ressler, B. Tomlin, C.N. Davids, C.J. Lister, and W.B. Walters, *Phys. Rev. C*57, 2259 (1998).
- [11] D. Bucurescu, C.A. Ur, D. Bazzacco, C. Rossi-Alvarez, P. Spolaore, C.M. Petrache, M. Ionescu-Bujor, S. Lunardi, N.H. Medina, D.R. Napoli, M. De Poli, G. de Angelis, F. Brandolini, A. Gadea, P. Pavan, and G.F. Segato, *Z. Phys. A*352, 361 (1995).
- [12] S.D. Paul, H.C. Jain, S. Chattopadhyay, M.L. Jhingan, and J.A. Sheikh, *Phys. Rev. C*51, 2959 (1995).
- [13] H. Schatz, A. Aprahamian, J. Görres, M. Wiescher, T. Rauscher, J.F. Rembeges, F.-K. Thielemann, B. Pfeiffer, P. Möller, K.-L. Kratz, H. Herndl, B.A. Brown and H. Rebel, *Phys. Rep.* 294, 167 (1998).
- [14] J. Garces Narro, C. Longour, P.H. Regan, B. Blank, C.J. Pearson, M. Lewitowicz, C. Miehe, W. Gelletly, D. Appelbe, L. Axelsson, A.M. Bruce, W.N. Catford, C. Chandler, R.M. Clark, D.M. Cullen, S. Czajkowski, J.M. Daugas, P. Dessagne, A. Fleury, L. Frankland, J. Giovinazzo, B. Greenhalgh, R. Grzywacz, M. Harder, K.L. Jones, N. Kelsall, T. Kszczot, R.D. Page, A.T. Reed, O. Sorlin, and R. Wadsworth, *Phys. Rev. C*63, 044307 (2001).
- [15] J. Döring, D. Pantelica, A. Petrovici, B.R.S. Babu, J.H. Hamilton, J. Kormicki, Q.H. Lu, A.V. Ramayya, O.J. Tekyi-Mensah, and S.L. Tabor, *Phys. Rev. C*57, 97 (1998).
- [16] A. Petrovici, K.W. Schmid, and A. Faessler, *Nucl. Phys. A*647, 197 (1999).
- [17] E. Caurier, A.P. Zuker, A. Poves, and G. Martínez-Pinedo, *Phys. Rev. C*50 (1994) 225.
- [18] K. Hara and Y. Sun, *Int. J. Mod. Phys. E*4, 637 (1995).
- [19] K. Hara and Y. Sun, *Nucl. Phys. A*531, 221 (1991).

- [20] R. Palit, J. A. Sheikh, Y. Sun, and H. C. Jain, Nucl. Phys. A686 141 (2001).
- [21] Y. Sun and J.A. Sheikh, Phys. Rev. C64, 031302 (2001).
- [22] Y. Sun and J.L. Egido, Nucl. Phys. A580, 1 (1994).
- [23] Y. Sun, J.-y. Zhang, M. Guidry, J. Meng, and S. Im, Phys. Rev. C62, 021601 (2000).
- [24] R. Zheng, S. Zhu, N. Cheng, and J. Wen, Phys. Rev. C64, 014313 (2001).
- [25] S. Frauendorf and J.A. Sheikh, Nucl. Phys. A645, 509 (1999).

Table 1  
Parameters used in the PSM calculations

| Nuclei           | $\epsilon_2$ | $G_Q$ |
|------------------|--------------|-------|
| $^{72}\text{Br}$ | 0.295        | 0.16  |
| $^{74}\text{Br}$ | 0.295        | 0.16  |
| $^{74}\text{Rb}$ | 0.360        | 0.16  |
| $^{76}\text{Rb}$ | 0.290        | 0.16  |
| $^{78}\text{Rb}$ | 0.273        | 0.16  |
| $^{80}\text{Y}$  | 0.311        | 0.16  |
| $^{82}\text{Y}$  | 0.255        | 0.16  |

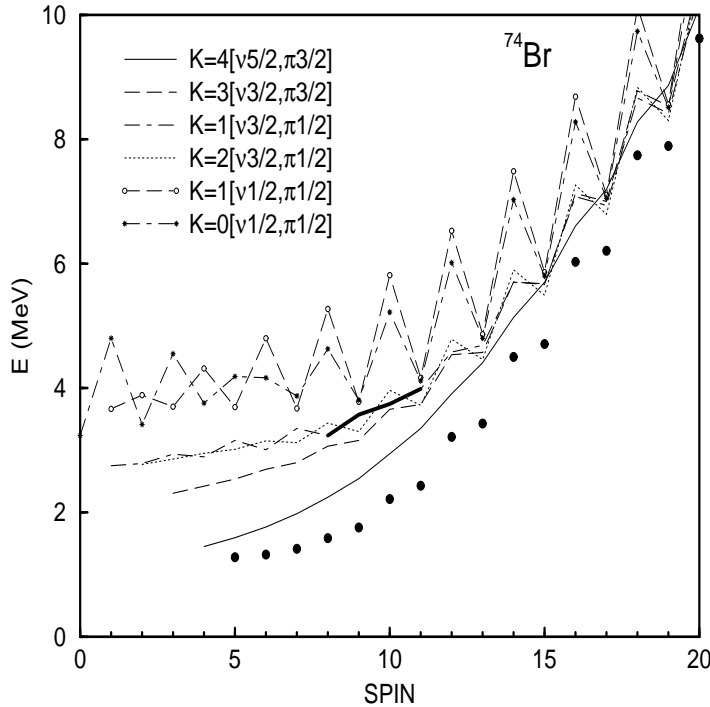


Fig. 1. A representative band diagram for  $^{74}\text{Br}$ . [For other isotopes, relative positions of the bands are different, reflecting different shell fillings.] Filled circles are the lowest states obtained after configuration mixing at each spin. Notice in particular the solid, bold curve at spin  $I = 8 - 11$ , which shows a self-inversion in that band.

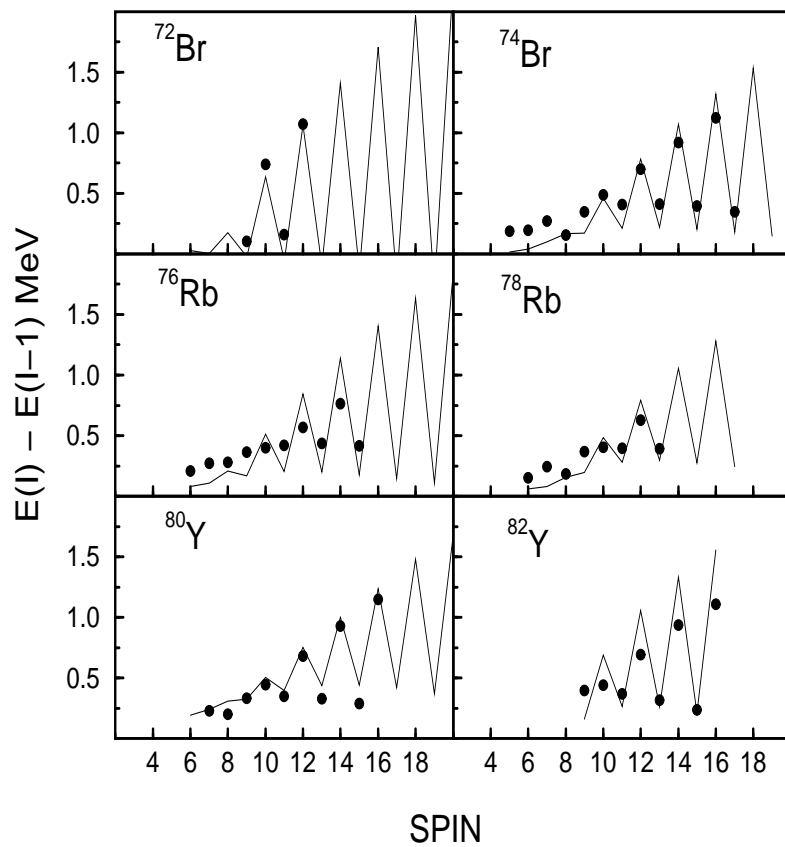


Fig. 2. Comparison of calculated transition energies (solid line) with experimental values (filled circle) for the positive parity bands of Br (data from [3–5]), Rb (data from [7–9]) and Y (data from [11,12]) isotopes.

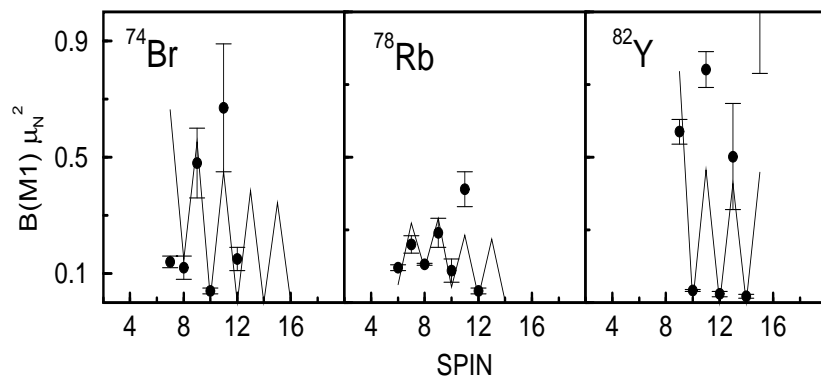


Fig. 3. Comparison of calculated  $B(M1)$  strengths (solid line) with the measured values (filled circle with error bar) for  $^{74}\text{Br}$ ,  $^{78}\text{Rb}$  and  $^{82}\text{Y}$  isotopes. Data are taken from [4,5,8,9,12]

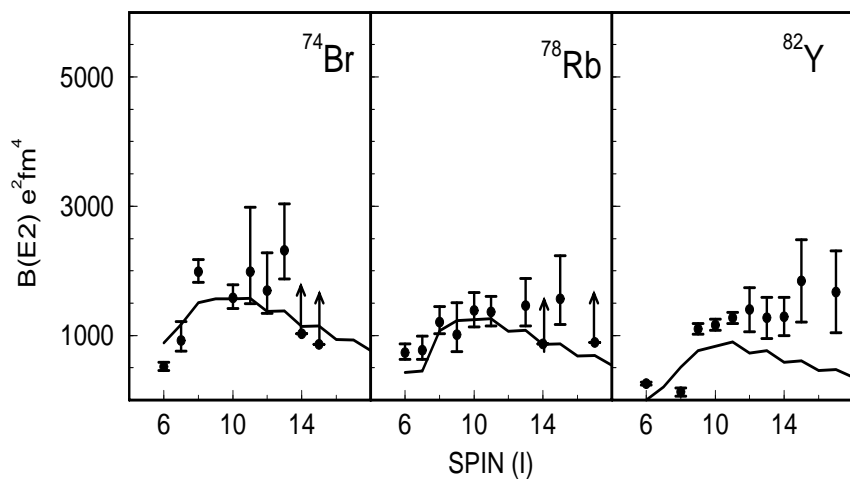


Fig. 4. Comparison of calculated  $B(E2)$  strengths (solid line) with experimental values (filled circle with error bar) for  $^{74}\text{Br}$ ,  $^{78}\text{Rb}$  and  $^{82}\text{Y}$  isotopes. Data are taken from [4,8,9,12].

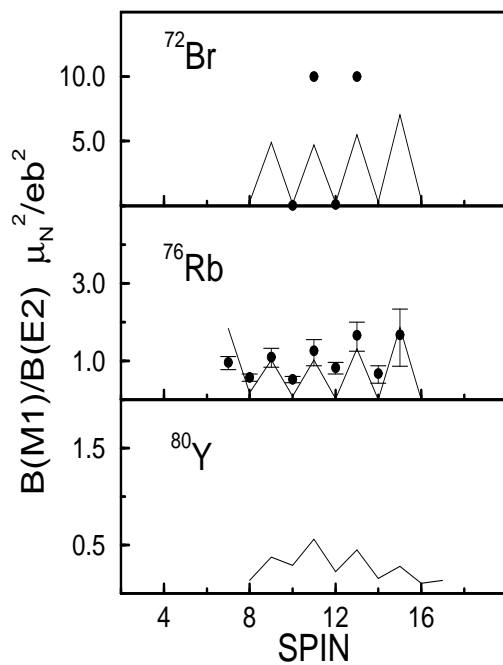


Fig. 5. Comparison of calculated ratio of  $B(\text{M1})$  to  $B(\text{E2})$  with experimental values (filled circle with error bar) for  $^{72}\text{Br}$ ,  $^{76}\text{Rb}$  and  $^{80}\text{Y}$  isotopes wherever data is available. Data are taken from [3,7,11].

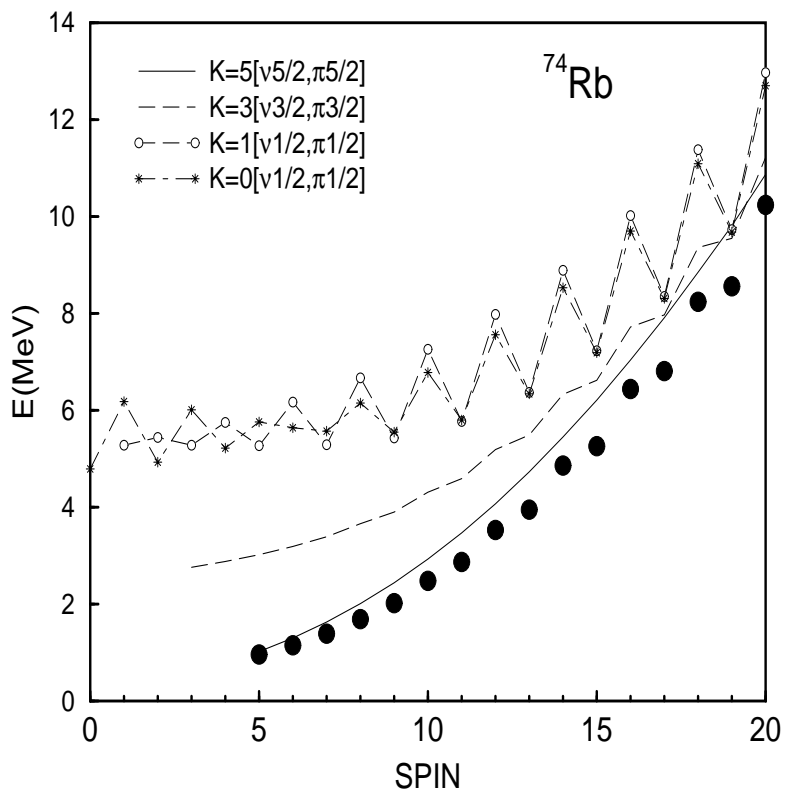


Fig. 6. Band diagram with 2-qp configurations for  $^{74}\text{Rb}$ . Filled circles are the lowest states obtained after configuration mixing at each spin.

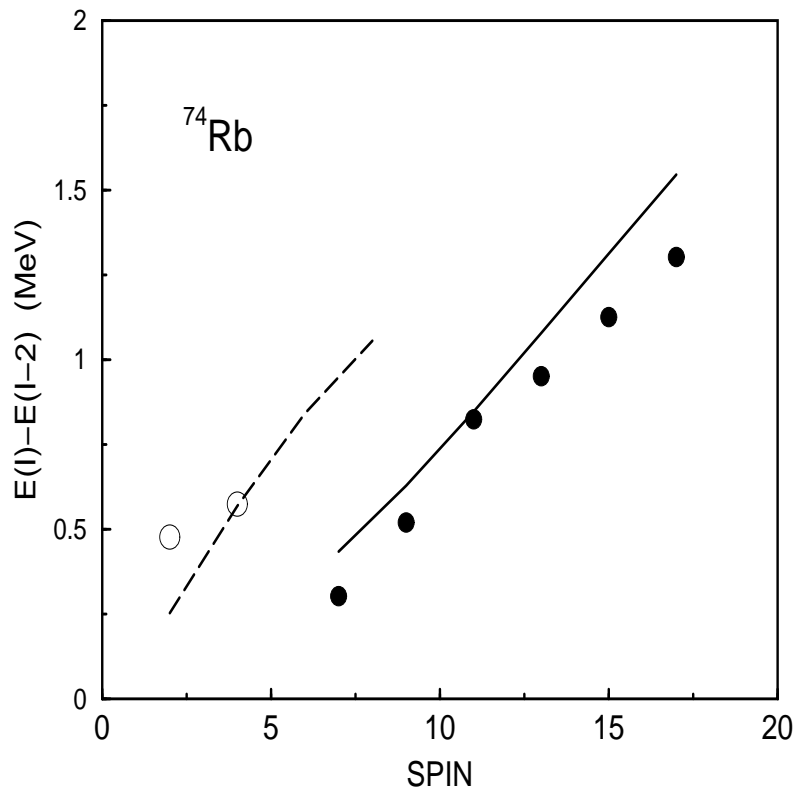


Fig. 7. Comparison of calculated transition energies (dashed line for 0-qp configuration and solid line for 2-qp configuration) with experimental values (open circle for the ground state band and filled circle for the excited band) for  $^{74}\text{Rb}$  (data from [6]).